



**PASSIVE RANGING USING INFRA-RED
ATMOSPHERIC ATTENUATION**

THESIS

Douglas J. Macdonald, Captain, USAF

AFIT/GAP/ENP/10-M09

**DEPARTMENT OF THE AIR FORCE
AIR UNIVERSITY**

AIR FORCE INSTITUTE OF TECHNOLOGY

Wright-Patterson Air Force Base, Ohio

APPROVED FOR PUBLIC RELEASE; DISTRIBUTION UNLIMITED

The views expressed in this thesis are those of the author and do not reflect the official policy or position of the United States Air Force, the Department of Defense, or the United States Government.

AFIT/GAP/ENP/10-M09

PASSIVE RANGING USING INFRA-RED ATMOSPHERIC ATTENUATION

THESIS

Presented to the Faculty

Department of Systems and Engineering Management

Graduate School of Engineering and Management

Air Force Institute of Technology

Air University

Air Education and Training Command

In Partial Fulfillment of the Requirements for the
Degree of Master of Science in Engineering and Environmental Management

Douglas J. Macdonald, BS

Captain, USAF

March 2010

APPROVED FOR PUBLIC RELEASE; DISTRIBUTION IS UNLIMITED.

PASSIVE RANGING USING INFRA-RED
ATMOSPHERIC ATTENUATION

Douglas J. Macdonald, BS
Captain, USAF

Approved:

_____/signed_____
Lt Col Michael R. Hawks (Chairman)

Date

_____/signed_____
Glenn P. Perram, PhD (Member)

Date

_____/signed_____
Kevin C. Gross, PhD (Member)

Date

Abstract

Methods of estimating range to an emissive target based on the depth of an atmospheric absorption band are demonstrated. The present work uses measurements of the CO₂ absorption band centered at 2.0 μm where signal-to-background ratios are maximum for many applications. Model results, based on high-resolution transmission molecular absorption (HITRAN) database cross sections, are used to predict range accuracy at ranges of up to 50 km and are compared with short range (<5km) experimental results. The spectra of 23 high explosive events were used to validate the model. Using the assumption of a blackbody spectrum, extracted ranges consistently underestimated the true range by approximately 13%. By incorporating the stoichiometry of the fireball from previous research and using particulate contribution as a parameter, the error for the range estimates could be reduced to 3%.

Acknowledgments

I would like to express my sincere appreciation to my research advisor, Lt Col Michael Hawks. His guidance on things both research and career related, as well as his sense of humor, helped keep me focused throughout this effort and keep me off the streets. I would also like to thank my sponsor, John Florio, from the National Air and Space Intelligence Center for his guidance and support of this effort.

I would also like to thank my committee members, Drs. Glen Perram and Kevin Gross. A significant amount of code used in this study was either created by Dr. Gross or inspired by various discussions with him during non-office hours. His willingness to take time out of his schedule to be a mentor for this effort had a tremendous impact on the quality of this research. The experience and insight provided by Dr. Perram was invaluable and it is an honor to have such a well respected individual on my committee. The assistance provided by Mr. Greg Smith, and Mr. Jeremy Pitz was also greatly appreciated.

To my friends and colleagues, thank you for all the support you have given me. Your constant cheer and support helped to keep me fresh and motivated.

Finally I would like to express my sincere appreciation for the love and support from my family. Through every milestone and accomplishment, they have always been there to cheer me on and give me the confidence I need. They mean the world to me.

Douglas J. Macdonald

Table of Contents

	Page
Abstract	v
Acknowledgments.....	vi
List of Figures	ix
List of Tables	xii
I. Introduction	1
Motivation	1
Problem Statement	1
Overview	2
II. Background	3
Band Ratio Method	3
Band Averaged Absorption.....	4
Advanced Monocular Passive Ranging.....	6
Summary	9
III. Approach.....	10
Theory	10
Discussion of the CO ₂ Band at 2 μm	14
IV. Experimental Setup.....	17
Introduction	17
Radiant Brass.....	18
Eglin Test	20
V. Analysis and Results	21
Introduction	21
Algorithm	21
Correcting for H ₂ O	24
Results	26
Accounting for Spectrally Selective Emission.....	27
Error Analysis	36
Discussion	40

	Page
VI. Conclusion	41
Future Work	42
Final Remarks	42
Appendix A. Pre-Processing Algorithm	44
Appendix B. Instrument Line Shape Algorithm	45
Appendix C. Water Correction Algorithm.....	48
Appendix D. Continuum Factor Optimization Routine.....	49
Appendix E. CO ₂ Optimization Routine.....	51
Bibliography	53

List of Figures

Figure	Page
1. Normalized blackbody curves for 300K atmospheric radiation and 6000K solar radiation. Highlighted area indicates the spectral region investigated by this study.....	2
2. Diagram of simplified radiative transfer scenario.	11
3. Comparison of CO ₂ and H ₂ O cross section at 300k. The CO ₂ cross section is weighted by 384 parts per million by volume (ppmv) and H ₂ O is weighted by 5000 ppmv (0.5% by volume).....	14
4. Curves of growth for the 2.0 μm CO ₂ band illustrating the advantage of using a downward-looking sensor. The transmittance for a downward-viewing angle was derived using an exponential atmosphere.	16
5. % Error in range versus range for two different viewing scenarios. Curves were generated assuming the error in measured transmittance is held at +/- 0.01.	16
6. (Top) View of target area from the observation tower. Events occurred near the dark mound in the distance. (Bottom) Layout of events. Circles represent event locations and the sensor was placed at the west tower.	19
7. Layout of Eglin test.....	20
8. (Top Left) Multiple frames of data are input into the algorithm. The data shown in this plot is from a Radiant Brass high explosive event. (Top Right) For each frame, a baseline is calculated from the out-of-band signal. (Bottom) This baseline is divided from the total signal for each frame, yielding the transmittance spectrum.....	22
9. (Top) Comparison of observed spectrum and model for typical Radiant Brass data. (Bottom) The same comparison, only for a different high explosive event at higher resolution.....	24
10. (Left) Comparison of observed spectrum for high explosive data and model for H ₂ O band at 2615-2730 cm ⁻¹ . (Right) Comparison for a different high explosive event at greater resolution.....	25

11. (Left) Optimized transmission model which accounts for water absorption. (Right) transmission model which does not account for water absorption.....	25
12. Results from Radiant Brass data. A significant amount of systematic error was observed with range estimates consistently underestimating the true range.....	26
13. Comparison of CO ₂ and H ₂ O cross sections at 1000k.....	27
14. Model source spectra for different continuum factors ϵ . Spectra were generated assuming the emitter had a spatial extent of 10 m and consisted of particulate, CO ₂ , and H ₂ O at 1000K, with both concentrations at 10 ¹⁷ molecules/cm ³ . The spectral regions used for passive ranging in this study are located at 4820-4885 and 4935-5010 cm ⁻¹	28
15. Simulated transmittance spectrum using different continuum factors for the source and showing ‘between band’ data.....	29
16. A small emission feature is consistently observed in the region between the two atmospheric absorption bands.....	31
17. Optimization result for continuum factor using data from Radiant Brass between the red and blue regions of the CO ₂ absorption band. In this example, the continuum factor ϵ was computed to be 0.96.	32
18. Comparison of optimization results which accounted for ϵ and those that did not. (Top Left) Two-band fit that did not take ϵ into account. (Top Right) Two-band fit which did take ϵ into account. (Bottom left) Red band fit which did not take ϵ into account. (Bottom Right) Red band fit which did take ϵ into account. While there was no visible difference in the quality of the model fits, the bottom right optimization was the only one to predict range within 2%.....	34
19. Radiant Brass results taking ϵ into account.	35
20. Curves of growth as calculated by the algorithm for different continuum factors ϵ . These curves were generated by simulating the observed signal using different values for ϵ and using the algorithm to compute a transmittance spectrum. This computed transmittance spectrum was then used to develop the curves of growth.....	38

21. Error in range as a function of range for different errors in transmittance. Even small errors in transmittance can produce large errors in range estimates 39

List of Tables

Table	Page
1. Range Estimates for Eglin Data.....	26
2. Range estimates for Eglin test taking ϵ into account.	35
3. Sources of error with their effect on pathlength. Assumed values for temperature and pressure were taken from on-site measurements. The variation in ppmv is due to seasonal changes.	37

PASSIVE RANGING USING INFRA-RED ATMOSPHERIC ATTENUATION

I. Introduction

Motivation

Many military applications require a range to target. One way this is accomplished is to use an active sensor such as radar. The drawback to using radar is that it alerts the adversary to the location of the sensor being used. Targets can also be acquired passively through both imaging and non-imaging photosensitive devices. Nearly all passive techniques however only give an azimuth and elevation to target. In order to actually acquire a range, triangulation would be needed, which requires multiple sensors at different locations with favorable viewing geometry. If range could be determined with a passive technique, a host of additional information could be derived from a single platform. This additional information would include latitude-longitude coordinates, altitude, velocity, aspect angle, and target performance. Examples of the military applications where this information would be useful include ISR platforms, missile defense platforms, and missile early warning systems.

Problem Statement

This thesis investigates how atmospheric attenuation of a signal can be used to determine range. A method that does not require a calibrated instrument, prior knowledge of the target, or precise measurements of multiple atmospheric parameters is advantageous since it enable range estimates to be performed real time. While dependence on local atmospheric conditions is unavoidable, a solution that depends only on a limited number of parameters such as temperature, pressure, latitude, and time of

year will be viable. As a consequence of these objectives, the scope of this study will be limited to targets whose spectra are dominated by continuum emission.

Overview

The main portion of the electromagnetic spectrum that was investigated was the CO₂ absorption band at 2 μ m. This band has the advantage of being in a spectral region where background from both solar radiation and atmospheric radiation are at a minimum:

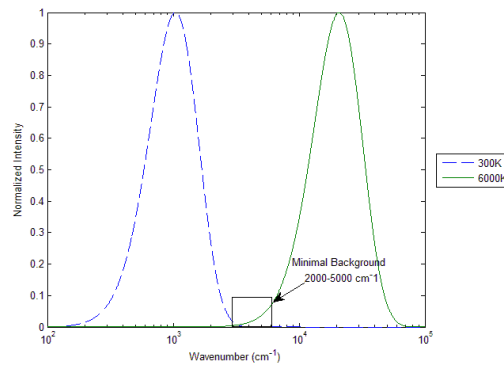


Figure 1: Normalized blackbody curves for 300K atmospheric radiation and 6000K solar radiation. Highlighted area indicates the spectral region investigated by this study.

Another advantage to using this band is that CO₂ concentrations are uniform and well known at altitudes of 20km and below [1]. This translates to better signal-to-background for any practical application of this technique. The drawback to using this region of the spectrum is that there are many absorption features due to atmospheric constituents other than CO₂, mainly H₂O. Another drawback to the CO₂ absorption band is that many targets of interest have CO₂ combustion products. This complicates estimates of atmospheric absorption in some targets due to both CO₂ emission and self attenuation from the target's combustion products.

II. Background

Band Ratio Method

Work done by S. Draper, W. Jeffrey, and C.K. Chuang involved taking the ratio of the intensities in two bands and using that value for passive ranging [2]. The two bands used for their technique were located at the red wing of the CO₂ band at 4.3 μm [2]. The model used depended upon various assumptions and required redundant knowledge of the target's spectrum as well as the attenuating medium. Either standard atmospheres or data collected from radiosondes were used to compute atmospheric parameters. Having to use *a priori* knowledge of the source spectrum introduces some difficulties to the problem. Not only is prior knowledge of the target a limiting factor, inaccuracies in the model for the source spectrum also lead to increased error. The bands used for this method were located in a spectral region where the optical depth of CO₂ was large, so any small deviation in the CO₂ concentrations used to develop the model would have had a significant impact on the actual spectrum. This was a problem experienced in later work that also tried to exploit the 4.3 μm region using predefined models [3].

The band ratio method was tested by Draper *et al.* using multiple data sets from different targets and from different platforms. One test involved data collected by a Fourier Transform Infra-Red Spectrometer (FTIR) with a resolution of 4 cm⁻¹ onboard a KC-135 at an altitude of 12.4 km on a solid rocket interceptor [2]. The target was launched 120 km from the sensor and ascended from an altitude of 2 km to 11 km during the 20-second flight time [2]. Using a Mid-latitude summer standard atmosphere, range estimates were off by 10% to 15%. In addition to the previously mentioned sources of error, there was also the possibility of a significant amount of random error due to the

low signal-to-noise ratio (S/N) of the data [2]. Another test utilized data collected by a DSP sensor on a space launch vehicle. Error in range estimates vary from negligible at altitudes < 8 km to approximately 20% at higher altitudes [2]. A “constant altitude signature assumption” [2] was used for this test so the approximation that the band ratio was independent of altitude likely led to systematic error in the calculated ranges. A third data set was collected on a Tactical Ballistic Missile (TBM) by an imaging spectrometer onboard an ARES aircraft [2]. Two data points were obtained for the range estimate. Using data from a radiosonde and correcting for instrument effects, the calculated range error for the two points was held to less than 5% [2].

Band Averaged Absorption

Another method developed at AFIT by Hawks *et al.* involves modeling the band averaged absorption of a target using the O₂ (X→b) band at 762 nm [4]. This band has an important advantage since it is spectrally isolated from other absorption features in the atmosphere. This enabled the un-attenuated spectrum to be derived by interpolating the data outside the absorption band rather than having to use a model and other prerequisite knowledge of the target. Another advantage to using O₂ is that its concentration is very uniform, well known, and is not strongly dependant on local weather conditions [4],[1]. This transition is also very weak so there is a dynamic range in the absorption, even at very long distances. Finally, much of the oxygen in targets of interest is consumed in a combustion process. As a result, contributions to the spectrum due to emission or self-attenuation of O₂ in the target are negligible compared to the continuum contributions. This reduces errors in the estimate of the target’s signal within the absorption band from the out-of-band interpolation. The main drawback to this method is that it lies just

outside the visible region of the spectrum where there is a significant amount of solar radiation and scattering. This increases the need for an accurate way of computing the background so that it can be subtracted from the signal. Also, since the signal to background is reduced, the target needs to be hotter in order to produce enough photons at this wavelength to be detected at longer ranges.

Range was estimated by Hawks by developing a model for the band-averaged absorption known as the curve of growth [4]. Range was interpolated from this curve using the experimentally derived band averaged absorption [4]. From Beer's law, the monochromatic absorption by a medium over some path of length L is given by

$$A(\omega, L) \equiv 1 - \frac{I(\omega, L)}{I(\omega, 0)} = 1 - \exp\left(-\int_0^L \sigma(\omega, l) N(l) dl\right) \quad (1)$$

where l is the distance from the target to the sensor, I is the intensity of the target at some distance l and wavenumber ω , N is the concentration, and σ is the cross section. The band integrated absorption is defined as follows:

$$\bar{A}(L) \equiv \frac{1}{\Delta\omega} \int_{\Delta\omega} A(\omega, L) d\omega \quad (2)$$

This equation describes the curve of growth, or a plot of \bar{A} as a function of L , which is very different from an exponential Beer's law curve for monochromatic attenuation. For this method, $\Delta\omega$ was chosen such that it spanned the entire O_2 band. This reduced the dependence of absorption on the ro-vibrational distribution (and hence the temperature) of the attenuating medium. The absorption for the experimental data was calculated using the following equation:

$$A(\omega) = 1 - \frac{I_{measured}(\omega)}{I_{baseline}(\omega)} \quad (3)$$

Where $I_{baseline}$ is the un-attenuated intensity of the source derived from the out of band data.

This method was validated by Hawks using a halogen lamp and a rocket motor test[4]. A curve of growth for the halogen lamp was empirically derived by taking multiple measurements of the spectrum up to 200 m using a Bomem MR-254 FTIR [4]. On a different day, the target was placed at 36.6 m and its spectrum was measured using various detector configurations [4]. The computed range was 37.1 m which was within 1.3% of the actual range [4]. This estimate was further refined to within 0.4% by adjusting the concentrations on the different days using only the temperature and the ideal gas law [4]. There was no apparent correlation between the resolution used and the range estimate [4]. For the rocket motor test, the same spectrometer was used and the target was located at a range of 2.825 km [4]. Again, using the local temperature and the ideal gas law an O₂ concentration was derived [4]. The range estimate for this test was 2.811 km, which was within 0.5% of the actual value [4]. For this target, only the R-branch of the spectrum was used to compute the absorption [4]. This was because there was a strong potassium line in the signature near the P-branch is location [4].

Advanced Monocular Passive Ranging

A third technique that has been investigated by G. Scriven and N. Gat is Advanced Monocular Passive Ranging (A-MPR) [5]. A-MPR is a technique that accomplishes a least squares fit between the observed intensity of the sensor and a parameterized model. The target's spectrum is computed using both the Standard Plume

Flowfield and Standard Plume Ultra Violet Radiation Code (SPF/SPURC) [5]. The inputs to SPF/SPURC are assumed to be known and are not parameters in the model [5]. The atmospheric profile is developed by letting pressure, temperature, humidity, etc. be parameters in the least squares fit [5]. The temperature profile is assumed to be given by the following eigenvalue equation:

$$\mathbf{T} \approx c_1 \cdot \mathbf{E}_I + \mathbf{M} \quad (4)$$

where \mathbf{E}_I is some temperature profile (a vector containing information on temperature at several altitudes) and \mathbf{M} is a vector the same length of \mathbf{E}_I but with all values set to the mean of \mathbf{E}_I [5]. The profile \mathbf{E}_I was selected by choosing one of the temperature profiles already built into MODTRAN which most closely resembled local conditions [5].

Pressure was modeled in the following manner:

$$P(h) = P_0 \cdot \exp\left(-\frac{g}{R} \int_{h_0}^h \frac{dh}{T}\right) = P_{hs} \cdot \exp\left(-\frac{g}{R} \int_{hs}^h \frac{dh}{T}\right) \quad (5)$$

where h_0 is ground elevation, hs is the height of the sensor, h is the height of the target, g is the gravitational constant, and R is the gas constant [5]. Humidity is then computed from these values for temperature and pressure [5]. As a result, temperature, pressure, and humidity profiles are modeled using only one parameter, c_1 . Ozone is also modeled using an eigenvalue approach, similar to how the temperature profile was modeled [5]. Finally, CO_2 concentration is set to a constant value of around 370 ppmv [5]. Using this approach, the overall atmosphere is modeled using only two parameters, one for the temperature profile and the other for the ozone profile.

One demonstration of A-MPR by Scriven *et al.* has been with a static rocket motor test [3]. An imaging spectrometer was used to collect the data. The imaging spectrometer operated between 1.8 and 5 μm , had a 6.3 nm resolution, and a 16x16 Focal Plane Array (FPA) [5]. A filter was put in place to eliminate the 2nd order diffraction in the instrument [5]. As a result, only the spectral region from 3 to 5 μm was used [5]. This limited the test to using just the 4.3 μm CO₂ absorption band [5]. The solid rocket motor was located at a distance of 2.8 km and burned for approximately 30 seconds [5]. Over the course of the burn, multiple range estimates were extracted. The predictions consistently underestimated the range at 2.0 km, which was roughly a 30% error [5]. Scriven *et al.* suggest this error is due to working in a region where the absorbing specie has a high optical depth. Comparison of the spatial extent of the plume between the model and data from the imaging spectrometer indicate the plume was wider than expected [5]. This affected the CO₂ concentration predicted by the model. Since CO₂ has such a high absorption cross section in the 4.3 μm region, any small variation in the concentration will have a large impact on the predicted spectrum.

Scriven *et al.* also applied A-MPR to historical data from a SCUD-B launch. This data had information available in both the 2.0 and 4.3 μm regions [5]. Using the 4.3 μm region, errors in range estimates exceeded 100% in some cases whereas for the 2.0 μm region there was only about a 5% error [5]. This illustrated the difficulty of attaining accuracy when using the 4.3 μm region.

A space launch was also used by Scriven *et al.* to validate A-MPR. The same imaging spectrometer used for the solid rocket motor test was used for this launch [5]. Due to problems tracking the launch, only about 12 seconds of data were used for range

extraction [5]. During this time, the slant range to the target was approximately 30 km [5]. Real time estimates of the range were off by as much as 35% in some cases [5]. These estimates used data from 1.97 – 2.15 μm [5]. During post-mission processing it was found that this error could be reduced to around 11% using a narrower spectral region which ranged from 1.99-2.05 μm [5]. It was proposed by Scriven *et al.* that the main source of error came from discrepancies between the plume model and the actual signature. For future work, development of a method less dependent on model target signatures and more dependent on the emission spectra for known gaseous constituents in the plume was suggested.

Summary

This study has built on the lessons learned from previous attempts at passive ranging. Since there have been difficulties with trying to use a model for the source signature, this has been avoided. Instead, the method presented in this thesis attempts to derive the source spectrum from the observed intensity as was done in the research by Hawks. One major drawback to using the O_2 transition at 762 nm however is the amount of background that needs to be removed from the signal. Focusing on the 2000 – 5000 cm^{-1} region enables range to be determined with dimmer targets, regardless of time of day or the scene in the sensor's field of view (FOV). There have also been complications in previous work which used spectral regions where there were large absorption cross sections. For this thesis, only regions that have small cross sections were investigated. This allowed for greater dynamic range in absorption as well as reducing error introduced by variations in molecular concentrations at the source.

III. Approach

Theory

The fundamental equation used for any radiative transfer problem is known as Schwarzschild's Equation [6]:

$$I = I_0 e^{-\tau} + \int_0^{\tau} B \cdot e^{-\tau'} d\tau' \quad , \quad (6)$$

where I_0 is the intensity of some source, B is the Planck blackbody function of the source, and I is the apparent intensity of the source observed by some detector at an optical depth of τ . Optical depth is defined as follows:

$$\tau \equiv \int_0^s N \sigma ds \quad , \quad (7)$$

where N is the number density of attenuating molecule, σ is the absorption cross section of that molecule, and s is the path length from source to detector. Equation (6) was derived using Kirchhoff's Law [6] which states emissivity and absorptivity are equal, in other words things emit the same amount of radiation as they absorb. Kirchhoff's Law assumes that the attenuating medium is in local thermodynamic equilibrium (LTE) with the radiation field. In order to develop a method independent of plume models or similar types of *a priori* knowledge, some simplifying assumptions had to be made. Figure 2 shows a diagram depicting the simplified scenario which was used to develop the method presented in this study:

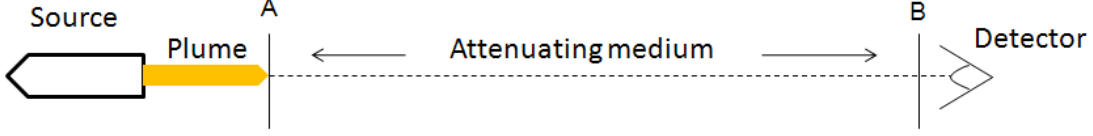


Figure 2: Diagram of simplified radiative transfer scenario.

First, the intensity observed just outside the plume will be investigated. This location will be referred to as point A and the location of the detector will be referred to as point B. From equation (6), the apparent intensity at point A is given by:

$$I_A = \Omega_{eng} B_{eng} e^{-\tau_{plume}} + \Omega_{plume} \int_0^{\tau_{plume}} B_{plume} e^{-\tau'} d\tau' \quad , \quad (8)$$

where B_{eng} and B_{plume} are the Planck blackbody functions of the hot engine parts and plume respectively, Ω represents some aspect angle dependence of those intensities, τ_{plume} is the optical depth of the plume, and τ' is the optical depth of the plume at some arbitrary point within the plume. As will be shown later, the method developed in this study is optimized for use on an air or space-borne platform looking downward. Since it is difficult to observe hot engine parts while looking downward on an ascending target, Ω_{eng} is assumed to be 0. Also, since Ω_{plume} is roughly constant over some measurement of I_A , it will be folded into B_{plume} as a constant amplitude factor.

The second term in equation (8) represents emission from the plume. The plume can be approximated as a series of discrete emitting shells. Within any given shell, B_{plume} will be approximately constant. Equation (8) can be broken up as follows:

$$\int_0^{\tau_{plume}} B_{plume} e^{-\tau'} d\tau' = \int_0^{\tau_{plume,1}} B_{plume} e^{-\tau'} d\tau' + \sum_{i=1} \int_{\tau_{plume,i}}^{\tau_{plume,i+1}} B_{plume} e^{-\tau'} d\tau' \quad , \quad (9)$$

where $\tau_{plume,i}$ is the optical depth of the i^{th} shell. Assuming an optically thick plume, the summation in equation (9) will be negligible compared to the integral over the first shell near the surface. Carrying out that integral yields the following result;

$$I_A = B_{plume} \left[-e^{-\tau'} \right]_0^{\tau_{plume,1}} \quad (10)$$

$$= B_{plume} \left(1 - e^{-\tau_{plume,1}} \right) \quad (11)$$

There are multiple different attenuating species that contribute to the optical depth. Suppose the plume consists of both particulate and a single emitting gas species. The transmittance of the plume can then be broken down in the following manner:

$$e^{-\tau_{plume,1}} = e^{-(N\sigma s)_{particulate}} \cdot e^{-(N\sigma s)_{gas}} \quad (12)$$

The functional form of τ presented in equation (12) assumes N and σ are independent of s , which would be valid under the previous assumption that the plume is at some constant temperature. Particulates do not generally exhibit a discrete emission spectrum since higher order energy level modes can be accessed by clumps of molecules as opposed to the discrete spectra of individual molecules. As a result, the particulate factor in equation (12) is roughly constant. Using this approximation, equation (11) can now be written as follows:

$$I_A = B_{plume} (1 - te^{-N\sigma s}) \quad (13)$$

Where t is the transmittance of particulates in the plume and the quantities in the exponents are for the gas in the plume. Since more interest is paid to the emissivity of particulates rather than their transmittance, t will be replaced by $1-\epsilon$. It is assumed that

the reflectivity of particulates in a plume can be neglected. Applying these changes to equation (13) yields the following:

$$I_A = B_{plume} \left[1 - (1 - \varepsilon) e^{-N\sigma s} \right] \quad (14)$$

Equation (14) represents the model that was used to approximate the source spectrum. For sufficiently small σ , the exponential quantity approaches 1 leaving the spectrum of a graybody.

The apparent intensity at the detector (point B) can now be determined by applying Schwarzschild's Equation one more time:

$$I_B = I_A e^{-\tau_{atmosphere}} + \textit{Background} \quad (15)$$

Where I_B is the apparent intensity at point B, $\tau_{atmosphere}$ is the optical depth of the attenuating medium, and the background term is due to thermal emission from the atmosphere or solar scattering. Assuming that the background is negligible (figure 1), this second term will go to 0.

At this point, the problem can be approached in two different ways. The first approach is to assume that the target is so optically thick due to particulate, or the emission cross sections for the emitting gasses are so small, that the source signal is essentially a graybody. Under these assumptions, no prior knowledge of the target will be needed since the source can be approximated by a polynomial fit to out of band spectral data. If neither of these assumptions hold, then some knowledge of the concentrations of gaseous emitters and plume extent (N and s respectively) will be required. A detailed explanation of these two methods is presented in Chapter V.

Discussion of the CO₂ Band at 2 μm

There are many reasons why the CO₂ absorption band at 2.0 μm is a propitious candidate for passive ranging. As stated earlier, this band is located in a spectral region where background is at a minimum. This band is also spectrally isolated from other atmospheric constituents with only a small contribution due to water. Additionally, this is a weak band, which is important, since it ensures that the transmittance does not saturate at long ranges. If the band stays weak at higher temperatures, it will also reduce the amount of gaseous emission features in the source spectrum. This is because higher concentrations and path lengths would be required to emit a sufficient amount of light to significantly affect the spectrum. Below is a plot showing the cross sections for both CO₂ and water at 300k and 1 atm. The plot was generated using information from the high-resolution transmission molecular absorption (HITRAN) database.

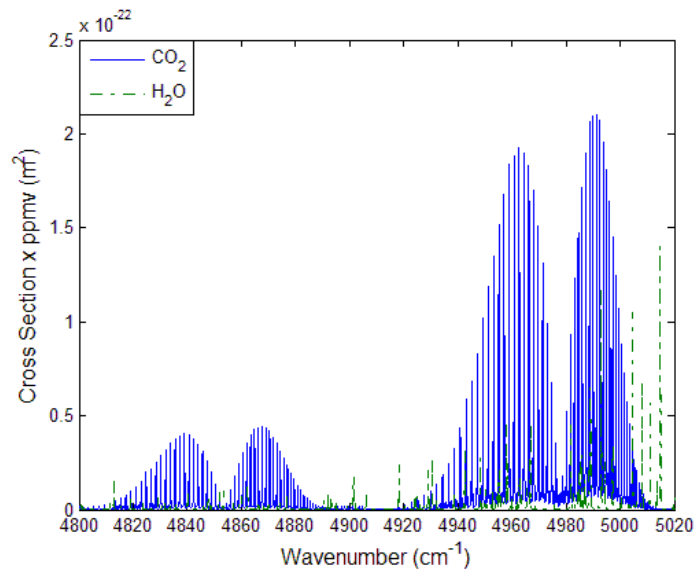


Figure 3: Comparison of CO₂ and H₂O cross section at 300k. The CO₂ cross section is weighted by 384 parts per million by volume (ppmv) and H₂O is weighted by 5000 ppmv (0.5% by volume).

Inspection of figure 3 shows that although the contribution due to water must be taken into account, it is only a small contribution and therefore may not need to be modeled to a high degree of accuracy. For example, error analysis done for experimental data taken at 4 km showed that if H₂O were neglected, there would be a 17% error in the range estimate. If the correction for transmittance due to water were within 20% from the true value, there would only be a 4% error in the estimated range (all other things equal). This is important since relative humidity can be highly variable over the typical pathlengths to be used for passive ranging. As was shown in the work done by Gat and Scriven [5], temperature, pressure, and relative humidity can be adequately modeled using only a few parameters. For the scope of this thesis and to reduce computational time, water was corrected for by determining concentration length using an isolated H₂O band at 2615 – 2730 cm⁻¹. The details of how this correction was made are presented in the Chapter V.

In order to determine whether or not this transition would saturate at longer ranges, curves of growth were generated for different viewing conditions. It was shown in the work by Scriven [3] that downward-looking platforms were more versatile at passive ranging than ground-based platforms. This is because a downward-looking platform can see through more atmospheric layers than a ground-based platform. Below are curves of growth for two different viewing geometries:

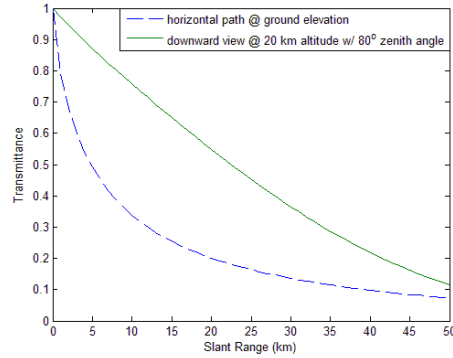


Figure 4: Curves of growth for the 2.0 μm CO_2 band illustrating the advantage of using a downward-looking sensor. The transmittance for a downward-viewing angle was derived using an exponential atmosphere.

Not only does the downward-viewing angle saturate at a longer range than the ground-to-ground view but it is also more linear. This is advantageous since the % error in range can be held to a minimum.

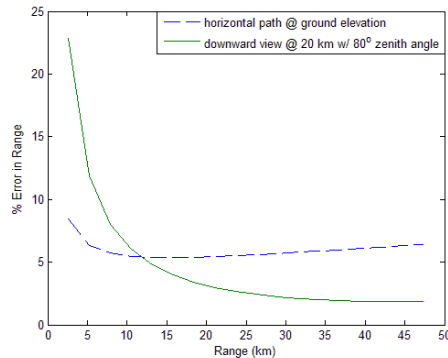


Figure 5: % Error in range versus range for two different viewing scenarios. Curves were generated assuming the error in measured transmittance is held at +/- 0.01.

The % error in range was derived by taking the derivative of the inverse of the curve of growth, multiplying by an assumed error in transmittance of 0.01, and then dividing by the range. It is clear that a downward looking viewing geometry is favorable compared to a horizontal view at low altitude for moderate to long ranges.

IV. Experimental Setup

Introduction

The scope of this study involves passively ranging targets with a spectrum dominated by continuum emission. Examples of such targets would include reentry vehicle and optically thick missile plumes such as from a solid rocket motor. An experiment intended to collect the spectrum of an Atlas V launch was carried out. The solid rocket boosters on the space launch vehicle were thought to produce a plume optically thick enough for this technique. Due to heavy fog however, no usable data was obtained. The spectrum of a reentry vehicle can very easily be reproduced using a blackbody (BB). Although blackbodies were available for this study, their aperture sizes were on the order of a few cm^2 . Consequently, there would not have been any usable signal from these blackbodies at ranges of a few km. As a result, historical data on high explosive detonations were used.

The algorithm used to estimate range was validated using 23 detonations from two different tests. Data on 21 of those detonations came from the Radiant Brass (RB) ground truth test at the Nevada Test Site (NTS). Radiant Brass was designed to test the capabilities of national assets in providing battlespace awareness. The ranges used in this test went from 3 – 5 km. A description of the experimental setup for Radiant Brass [7] was taken from Jay Orson's thesis and a test report by William and Sean Miller [8]. Data from the other two events were pulled from a similar test at Eglin Air Force Base. The goal of the Eglin test was to investigate the time evolution of detonation signatures. The explosives used had differing types of chemical composition. The signatures were

collected at a range of 315 m. Information regarding the experimental setup for this test was taken from a paper written by Joe Gordon [9].

Radiant Brass

The instrument used to collect data on this test was the Bomem MR-154 Fourier Transform Spectrometer (FTS). The FTS used both an HgCdTe and InSb detector. For this study, the primary source of data was the InSb detector. The spectral range of data collected was from 1800 to 6000 cm^{-1} . Since the main purpose of this test was to investigate the temporal evolution of the detonations, numerous trade-offs had to be made with regard to spectral resolution. These included using only one sweep direction of the Michelson interferometer and decreasing the MOPD. Most of the data were collected at 16 cm^{-1} resolution. A few datasets were collected with 4 cm^{-1} resolution. For the 16 cm^{-1} resolution data, the temporal resolution was 0.047 s. For the 4 cm^{-1} resolution data, the temporal resolution was 0.245 s. The optics used provided a 300 m field of view at 4 km. All internal aperture stops were set to 6.4 mm, which was the widest setting.

In order to accurately model CO_2 concentrations, temperature and pressure data are required. Temperature was measured using an Ertco whirling hygrometer/sling psychrometer. Pressure was measured using a Druck Model DPI 740 Precision Pressure Indicator. Relative humidity was calculated using a psychometric method [8]. Since relative humidity is highly variable with location those measurements were not used. Instead, water concentration length was determined from the spectrum by using the method outlined in the previous chapter.

The test was performed approximately 35 miles north-northwest of Fallon, Nevada. The elevation at this location is 4,000 ft above sea level. The range from sensor

to target varied from 3 to 5 km. The instruments were placed atop an observation tower and had an unobstructed view to the target. The figures on the following page are from Orson's thesis [7].

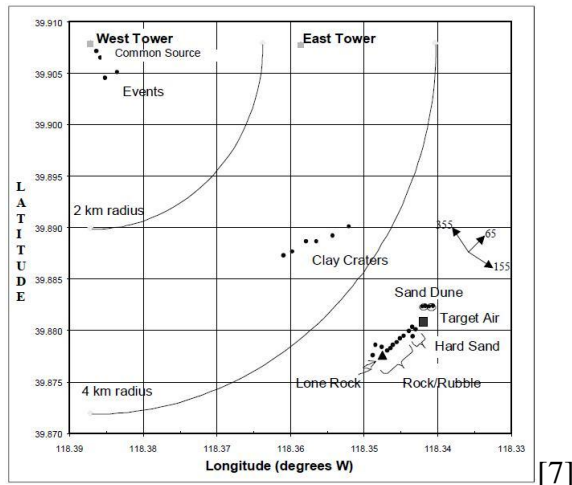


Figure 6: (Top) View of target area from the observation tower. Events occurred near the dark mound in the distance. (Bottom) Layout of events. Circles represent event locations and the sensor was placed at the west tower.

Although numerous blackbody calibrations were performed, they were not used for this study. Since the overall detector response is a slowly varying contribution to the observed spectra, it is eliminated when the out-of-band baseline is divided out from the signal. Therefore, no calibrations were needed for this technique to work.

Eglin Test

The primary instrument used on this test was the MR-254 (FTS). The FTS used for this test was also outfitted with an HgCdTe and InSb detector. Again, only data from the InSb detector was used. The spectral range of data collected was from 1800 to 10000 cm^{-1} . For this test, the data sets used had a spectral resolution of 8 cm^{-1} . At this resolution, the temporal resolution was 55 Hz. The FTS was fitted with a 76 mrad optic which corresponded to a 24 m diameter field of view at target.

The test was performed At Eglin Air Force Base, Florida. All experimental data was taken at a range of 315 m. Below is a diagram From Gordon's paper[9] depicting the experimental setup:

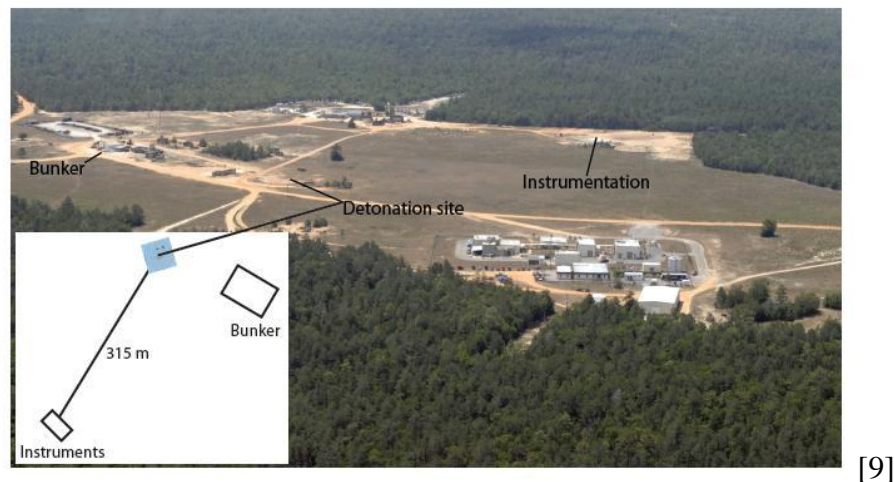


Figure 7: Layout of Eglin test.

V. Analysis and Results

Introduction

Between the data from Radiant Brass and Eglin, 23 high explosive events were used to validate the passive ranging method. An algorithm which computes the transmittance spectrum for these datasets assuming a graybody source was developed. The results for this method are provided. Another algorithm was then developed which took into account spectrally selective emission but required some knowledge of the target. The level of improvement for the spectrally selective method over the graybody method is presented. Error analysis was performed using the equation for transmittance given by Beer's law and the curves of growth.

Algorithm

The basic goal of the algorithm was to find a fit between the transmittance spectrum computed from the data and a parameterized model for the transmittance spectrum. A transmittance spectrum is derived from the data by interpolating the signal outside of the absorption band. This interpolated baseline is assumed to be the signal due to slowly varying contributions such as the blackbody source signal, detector response, and continuum factors. Assuming a graybody for the source ($\sigma_{gaseous\ emission} = 0$),

$$I_B \Big|_{out\ of\ band} = \epsilon B_{source} \quad . \quad (16)$$

A transmittance spectrum is derived by dividing this baseline from the data within the absorption band.

$$I_B = \epsilon B_{source} t_{atmosphere} \quad (17)$$

$$\Rightarrow t_{atmosphere} = I_B / I_{B, out\ of\ band} \quad . \quad (18)$$

The steps by which the algorithm takes to compute a transmittance spectrum are shown below. The order in which the steps are performed proceed clockwise starting from the top left.

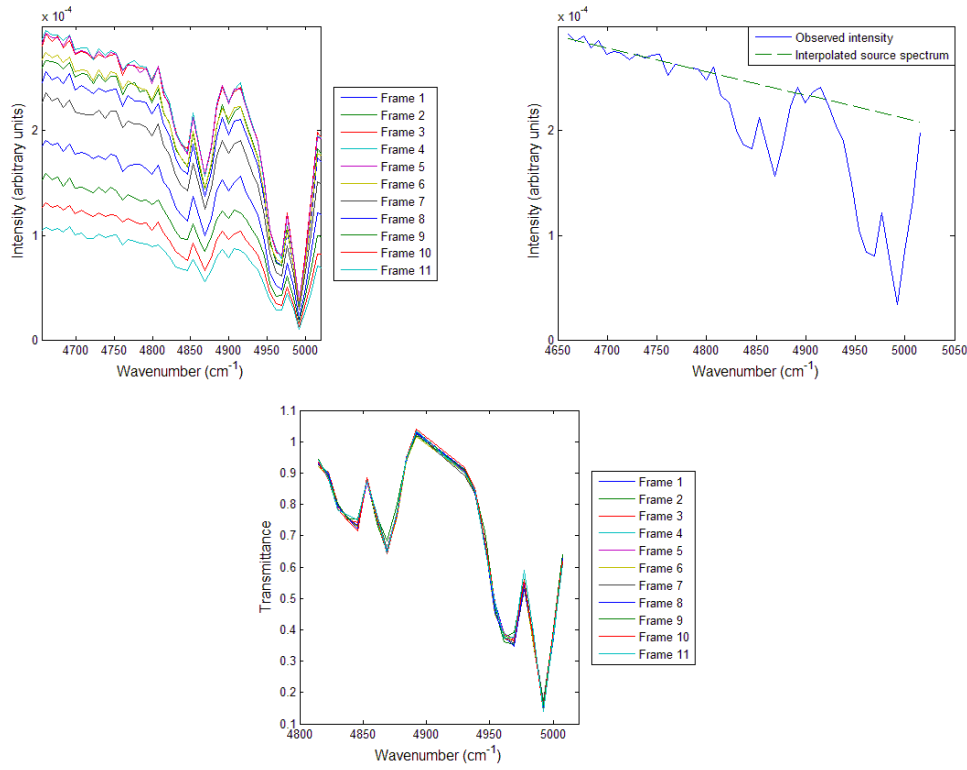


Figure 8: (Top Left) Multiple frames of data are input into the algorithm. The data shown in this plot is from a Radiant Brass high explosive event. (Top Right) For each frame, a baseline is calculated from the out-of-band signal. (Bottom) This baseline is divided from the total signal for each frame, yielding the transmittance spectrum.

The calculated transmittance spectrum is fit to a model based on Beer's law with pathlength as a parameter:

$$t_{atmosphere} = e^{-(N_{water}\sigma_{water} + N_{CO_2}\sigma_{CO_2})s} \quad (19)$$

$$= e^{-C.L \times \sigma_{water}(T,P) + N(T,P) \times \sigma_{CO_2}(T,P) \times s} \quad (20)$$

where $C.L.$ is a concentration length (equal to the product Ns). In the above equations, attenuation due to both CO_2 and H_2O is taken into account. The correction for water is detailed in a later section. For now, assume the concentration length and cross sections for water are known quantities. In order for pathlength to be decoupled from the concentration and cross sections of CO_2 , those values have to be known quantities. This is because concentration and cross sections all appear in the exponent of equation (20). The cross sections were taken from the HITRAN database. The concentration of air was computed using the ideal gas law and temperature and pressure measurements taken for each data set. CO_2 concentration was then calculated assuming 364 ppmv (the value for 1999). After all the above calculations are made, the only unknown parameter left in the exponent of equation (20) is pathlength. In order for a comparison to be made between the transmittance model and the observed data, instrument line shape (ILS) had to be taken into account. The experimental data was taken with an FTIR spectrometer. Therefore the measured spectrum depends upon the maximum optical path difference (MOPD) of the interferometer. Using MATLAB's built-in inverse Fourier transform function, the model transmittance spectrum was converted into an interferogram and multiplied by a rectangular line shape. The width of the rectangular line shape is equal to twice the MOPD that was used for the measurement. Taking the Fourier transform of this convolution returns the transmittance spectrum at a resolution which matches the data. The program which performed this correction for ILS was developed by Dr. Kevin Gross.

A 3-dimensional array containing the model transmittance spectrum for different values of pathlength was generated (transmittance vs. wavenumber and pathlength). A

function was created which applied 2-dimensional interpolation to this 3-dimensional array. The result is a function for the transmittance spectrum vs. pathlength. A built-in MATLAB Levenberg-Marquardt least squares technique was then used to perform a non-linear fit between this function and the data. Below are representative plots depicting the quality of those fits.

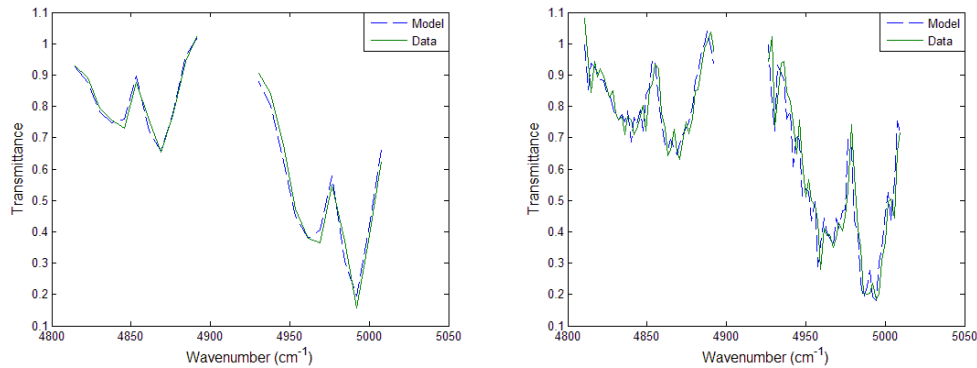


Figure 9: (Top) Comparison of observed spectrum and model for typical Radiant Brass data. (Bottom) The same comparison, only for a different high explosive event at higher resolution.

Correcting for H₂O

The concentration length for water in equation (20) was found by applying a similar least squares technique to the data located in an isolated water band at 2615-2730 cm⁻¹. A concentration length was computed and used to correct for water in the band at 4900 cm⁻¹.

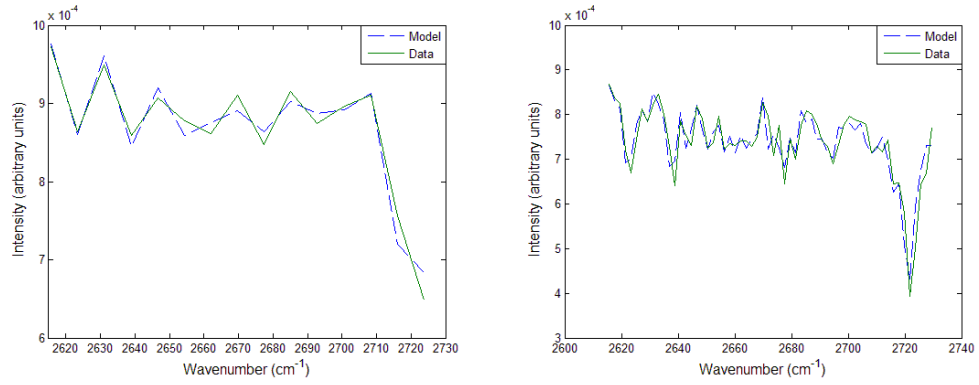


Figure 10: (Left) Comparison of observed spectrum for high explosive data and model for H₂O band at 2615-2730 cm⁻¹. (Right) Comparison for a different high explosive event at greater resolution.

A significant improvement in the quality of the model fits is observed when this concentration length is applied to equation (20). This is shown in the figures below:

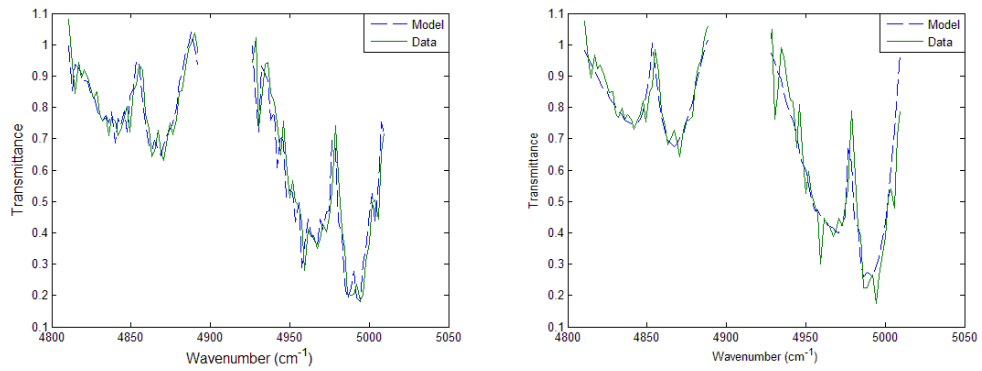


Figure 11: (Left) Optimized transmission model which accounts for water absorption. (Right) transmission model which does not account for water absorption.

Results

Figure 12 shows range estimates for Radiant Brass assuming a graybody source:

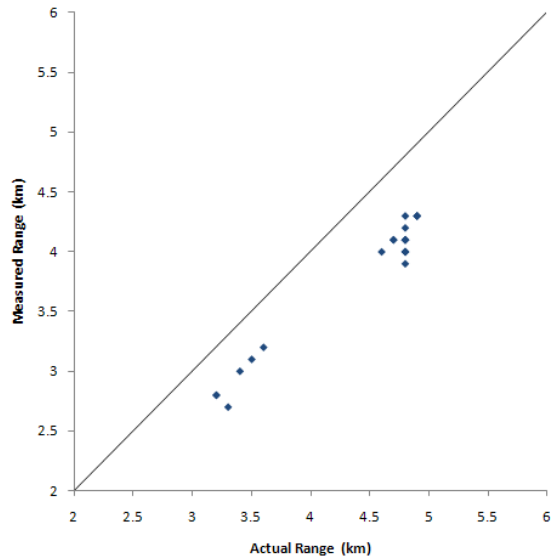


Figure 12: Results from Radiant Brass data. A significant amount of systematic error was observed with range estimates consistently underestimating the true range.

The mean error was 14% and the standard deviation for the error was approximately 2%. In all cases the algorithm consistently underestimated the range. Error introduced by emission within the absorption band would explain this systematic error. For the Eglin test, data from two events were extracted:

Table 1: Range Estimates for Eglin Data

Type	Estimated	Actual	% Error
Event 1	0.32	0.31	1
Event 2	0.33	0.31	2

In both cases for the Eglin test, there was a slight over-estimation in range. For both events, only a few frames of data were usable and the estimates fell within 2%.

Accounting for Spectrally Selective Emission

The method which has been developed up until this point has assumed that the target's spectrum could be adequately modeled using a graybody curve. Although this eliminated the need for *a priori* information on the target, this likely introduced systematic error from spectrally selective emission. This section will investigate a way of accounting for spectrally selective emission given certain assumptions of the target.

To see how spectrally selective emission affected range estimates, a model for the source spectrum was developed. This model is based on equation (14) which requires knowledge of the continuum factor ϵ , emission cross sections, emitter concentrations, and the spatial extent of the target. It was assumed that the only contributions to emission were due to CO_2 and H_2O . Below is a plot showing CO_2 and H_2O cross sections at 1000k, taken from the HITRAN high temperature database.

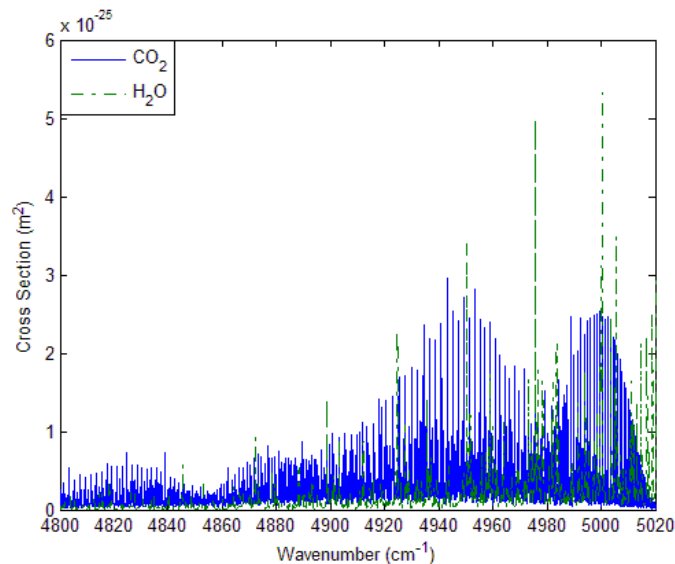


Figure 13: Comparison of CO_2 and H_2O cross sections at 1000k.

A plot of equation (14) for different values of the continuum factor ε is also shown below. The plot was generated using the high temperature cross sections, CO₂ and water concentrations of approximately 10^{17} molecules/cm³, and assuming a spherically symmetric emitter with a radius s of 10 m. The CO₂ and water concentrations were taken from a study by Dr. Kevin Gross of high explosive events [10].

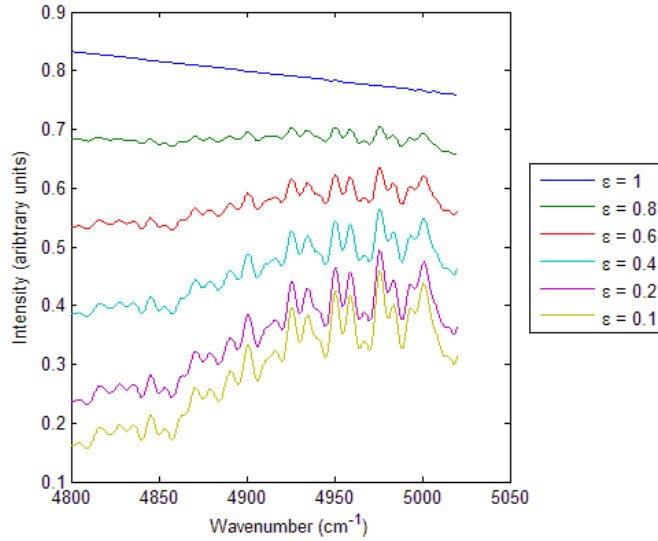


Figure 14: Model source spectra for different continuum factors ε . Spectra were generated assuming the emitter had a spatial extent of 10 m and consisted of particulate, CO₂, and H₂O at 1000K, with both concentrations at 10^{17} molecules/cm³. The spectral regions used for passive ranging in this study are located at 4820-4885 and 4935-5010 cm⁻¹.

The two spectral regions used for this study were located at 4820-4885 and 4935-5010 cm⁻¹. By inspection of figure 14, the red band (4820-4885 cm⁻¹) should provide a more accurate estimate than the blue band (4935-5010 cm⁻¹) since there is less spectrally selective emission. As expected, when the emissivity of the particulate decreases, the spectrum becomes more spectrally selective as the only emission features are those from gaseous constituents. However the signal also decreases as the continuum factor decreases since the CO₂ and H₂O have weak cross-sections in this spectral region.

Therefore it can be assumed that in order to receive a signal kilometers away in the first place, your spectrum must be dominated by continuum.

Below is a plot depicting the transmittance spectrum calculated by the algorithm using equation (14) to simulate the source signal with different continuum factors.

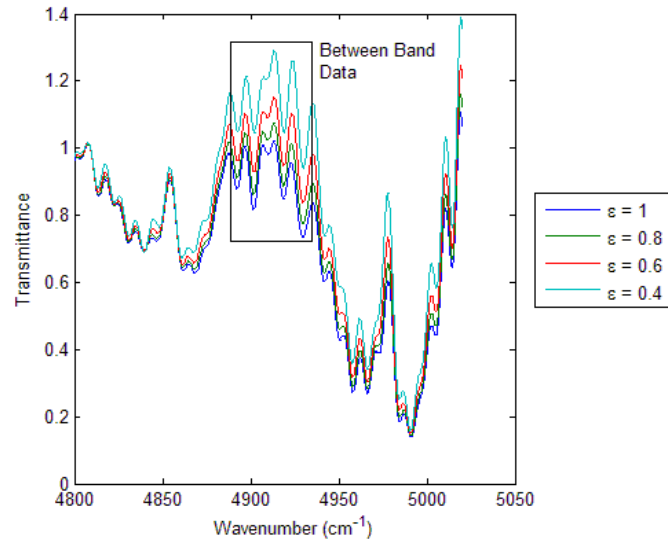


Figure 15: Simulated transmittance spectrum using different continuum factors for the source and showing ‘between band’ data.

As is evident from figure 15, the continuum factor has a significant impact on error in measured transmittance. Notably, there are no spectrally selective features which stand out within the absorption bands. Since the main differences between the different curves are the relative heights rather than spectral features, it is difficult to decouple emission and absorption by using just the data within the absorption bands. It is only between the absorption bands that differences in the continuum factor stand out. In this region the atmospheric transmittance is nearly 1, with only a small contribution due to water which we are treating as a known quantity. As a result, emission and absorption can be decoupled between the two absorption bands. Referring back to equations (14)

and (15), the apparent intensity observed by the detector (with background subtraction) is:

$$I_B = B_{source} \left[1 - (1 - \varepsilon) e^{-(N\sigma_s)_{source}} \right] t_{atmosphere} \quad . \quad (21)$$

At $4660 \text{ cm}^{-1} < \varpi < 4810 \text{ cm}^{-1}$, $t_{atmosphere}$ is approximately 1 and the emission cross section for the gaseous contribution to the source approaches 0. This leaves the signal observed in this region in a familiar format:

$$I_B \Big|_{4660 \text{ cm}^{-1} < \varpi < 4810 \text{ cm}^{-1}} = \varepsilon B_{source} \quad , \quad (22)$$

where ϖ denotes wavenumber. Between the red and the blue region of the absorption band, the atmospheric transmittance is still 1. However the emission cross sections of the source do not reach 0 since they are at a higher temperature and can access higher ro-vibrational levels than the relatively cold atmosphere. Thus the cross sections of the source extend into the region where the relatively cold CO₂ cross sections are still 0.

Therefore, the signal between the red and blue band is given by the following equation:

$$I_B \Big|_{4885 \text{ cm}^{-1} < \varpi < 4935 \text{ cm}^{-1}} = B_{source} \left[1 - (1 - \varepsilon) e^{-(N\sigma_s)_{source}} \right] \quad . \quad (23)$$

Dividing the baseline, equation (22), from the between-band data, equation (23), yields:

$$r = \frac{1}{\varepsilon} \left[1 - (1 - \varepsilon) e^{-(N\sigma_s)_{source}} \right] \quad , \quad (24)$$

where r is the ratio of the data between the absorption bands and the baseline that was interpolated from outside the absorption bands. Normally r would represent the calculated transmittance spectrum. Assuming a blackbody, ε will equal 1 which then reduces r to 1. This is the value for atmospheric transmittance in the region between the

two absorption bands. For $\varepsilon < 1$ (and $e^{-(N\sigma s)_{source}} < 1$), r becomes greater than 1. This would be expected since a transmittance of >1 would be measured if there was spectrally selective emission. The parameter ε was computed by fitting equation (24) to data between absorption bands divided by the baseline. The number density N was estimated to be 10^{17} molecules/cm³ based on research by Dr. Gross [10]. The cross sections σ for both CO₂ and water were taken from the high temperature HITRAN database assuming a temperature of 1000K. The spatial extent of the emitting species was assumed to be 10 m. Below is a plot of data from event 9 of Radiant Brass. The dashed line represents the baseline corresponding to equation (22).

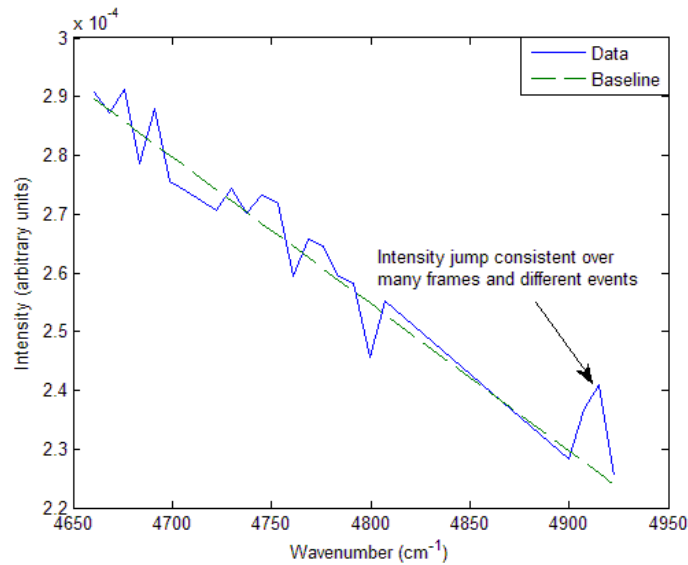


Figure 16: A small emission feature is consistently observed in the region between the two atmospheric absorption bands.

The spike observed in figure 19 was consistently observed over all 16 Radiant Brass events that were taken at 16 cm⁻¹ resolution. Events taken at 4 cm⁻¹ resolution also exhibited a rise, although the spectrum looked more like random band emission than a

single spike. On the following page is a plot showing the fit between r and the between band data:

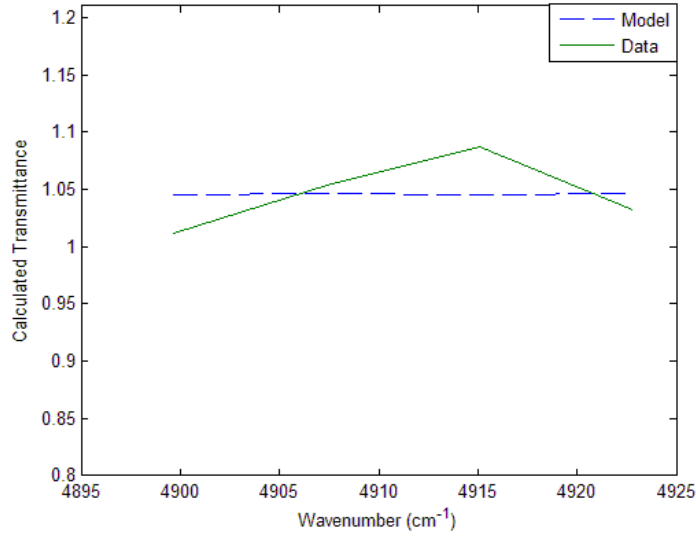


Figure 17: Optimization result for continuum factor using data from Radiant Brass between the red and blue regions of the CO₂ absorption band. In this example, the continuum factor ε was computed to be 0.96.

Possibilities as to why the model did not exactly match the data include using the wrong water or CO₂ concentration for the source, an incorrect spatial extent of the source, or emission due to a molecular specie that was unaccounted for. Nonetheless, reasonable results for the continuum factor were produced. For the data shown in figure 17, ε was calculated to be 0.96. Using this continuum factor, the model for the transmittance spectrum was modified in the following way:

$$\frac{I_{\text{within absorption band}}}{I_{\text{baseline}}} = r(\varepsilon) \cdot t(s) \quad (25)$$

where $t(s)$ is the transmittance spectrum derived earlier, given by equation (20). Using this value for ε , the range estimate for the event 9 was increased from 4.0 to 4.2 km (4.8

km actual). Even with this new value the error is still 13%. Unlike the original graybody method however, a significant difference was observed if just the red band was used. Using only the red band for the estimate, a range of 4.9 km was extracted. This translated to an error of 2%. The bias created when using the blue band could be due the approximation use to estimate the water emission. Since the effects due to water emission are more heavily weighted towards the blue region of the absorption band, this could explain the bias. The blue region could also be corrupted if there was some unaccounted for emitter. Both sources of bias would explain the imperfect match between r and the between-band data shown in figure 17. Since the correction for transmittance was small, it appeared range estimates using the red band was more susceptible to changes in transmittance. This could be due to the fact that the red band is the weaker absorption feature and is more susceptible to small changes in transmittance. This may be mitigated by the fact that there is less error introduced in this region. On the following page is a comparison between optimizations which did or did not account for ϵ .

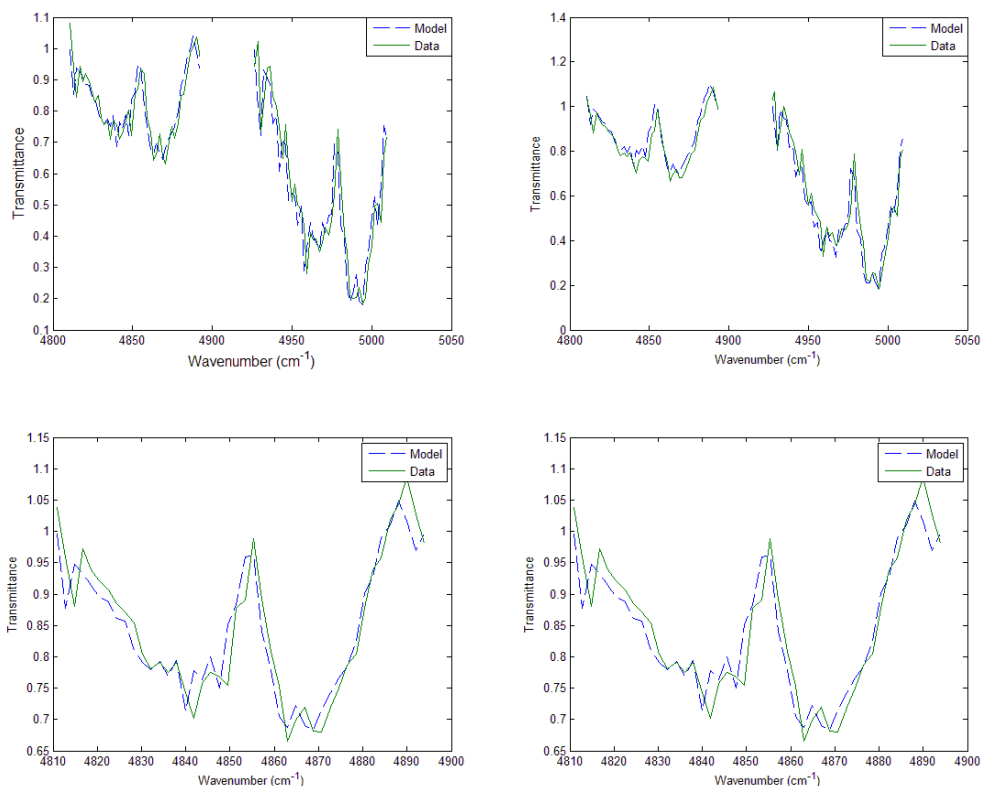


Figure 18: Comparison of optimization results which accounted for ε and those that did not. (Top Left) Two-band fit that did not take ε into account. (Top Right) Two-band fit which did take ε into account. (Bottom left) Red band fit which did not take ε into account. (Bottom Right) Red band fit which did take ε into account. While there was no visible difference in the quality of the model fits, the bottom right optimization was the only one to predict range within 2%.

By inspection of figure 18, there is no significant difference in the spectrum fit between using and not using ε . In fact, the differences in range estimates between the two-band methods which do and do not take into account ε are also small. It is only when using the red band that those differences are appreciable. On the following page is a figure which summarizes the results for the method which takes ε into account and uses only the red absorption band:

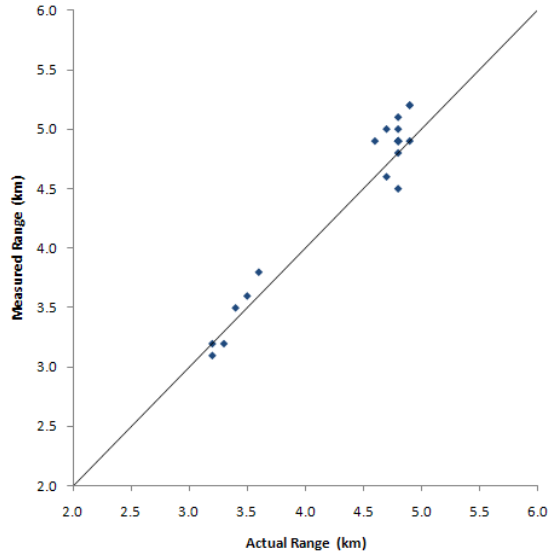


Figure 19: Radiant Brass results taking ϵ into account.

The mean error was 3.4% with no apparent systematic error. There also seemed to be a correlation between the continuum factor ϵ and the amount of explosives used. For events classified as large, the average value for ϵ was 0.98. For events classified as small, the average value of ϵ was 0.96. Events were classified according to the weight of the explosive material.

Results from the Eglin test were as follows:

Table 2: Range estimates for Eglin test taking ϵ into account.

Type	ϵ	2-Band Estimate (km)	Red-band Estimate (km)	Actual (km)	% Error for Red Band
Event 1	0.99	0.40	0.42	0.315	33
Event 2	0.99	0.35	0.24	0.315	24

It is not surprising that range estimates for the Eglin data are poor. The quality of the results using the graybody method was already suspect, since at this range the curve of

growth is very susceptible to errors in transmittance. It will be shown in the following section that in this region, uncertainties in transmittance of only 0.01 yield errors in range >20%. This issue is exacerbated for a method which only uses the red band since this absorption feature is very weak at ranges < 1km.

Error Analysis

Starting from Beer's law, the monochromatic transmittance can be calculated as follows:

$$t = e^{-N\sigma s} \quad (26)$$

where t is the transmittance, N is the number density of your attenuating specie, and s is the pathlength. Equation (26) assumes concentration and cross section are independent of pathlength. Solving for s and assuming σ is a known quantity, the error in pathlength as it relates to error in concentration can be derived:

$$s = \frac{-\ln(t)}{N\sigma} \quad (27)$$

$$\Delta s = \frac{\ln(t)}{N^2\sigma} \Delta N \quad (28)$$

$$= -\frac{N\sigma s}{N\sigma} \frac{\Delta N}{N} \quad (29)$$

$$\Rightarrow \frac{\Delta s}{s} = -\frac{\Delta N}{N} \quad (30)$$

Equation (30) shows that if N were overestimated by a certain percentage, s would be underestimated by that same percentage. Using the ideal gas law to compute N , errors in pathlength with respect to errors in temperature and pressure can also be derived:

$$N = \frac{P}{kT} ppmv_{CO_2} \times 10^{-6} \quad (31)$$

$$\Delta N = \frac{P}{kT} ppmv_{CO_2} \times 10^{-6} \left(\frac{\Delta P}{P} - \frac{\Delta T}{T} + \frac{\Delta ppmv_{CO_2}}{ppmv_{CO_2}} \right) \quad (32)$$

$$\frac{\Delta N}{N} = \left(\frac{\Delta P}{P} - \frac{\Delta T}{T} + \frac{\Delta ppmv_{CO_2}}{ppmv_{CO_2}} \right) \quad (33)$$

From equations (30) and (33), the magnitude of the error in range with respect to a given parameter is equal to the magnitude of error for that parameter.

Table 3: Sources of error with their effect on pathlength. Assumed values for temperature and pressure were taken from on-site measurements. The variation in ppmv is due to seasonal changes.

Parameter	Assumed Value	Error in pathlength
T (K)	273 ± 5	1.8%
P (Pa)	8.9 × 10 ⁵ ± 1 × 10 ³	0.1%
ppmv	367 ± 5	2.7%

As well as the sources of error above, there are other factors which contribute to the error.

One of those factors is absorption due to water. The difference between the band averaged absorption which takes into account water absorption, and the averaged absorption which does not, is 0.03 (an error in transmittance of 5%). By using the isolated water band to correct for H₂O concentration length, this error of 5% should be significantly reduced, as was show in figure 11.

Another major source of error is the presence of emission features within the absorption band. As was shown in figure 18, it is difficult to determine emission features

using only data within the absorption band. Neglecting emission altogether can significantly impact the results.

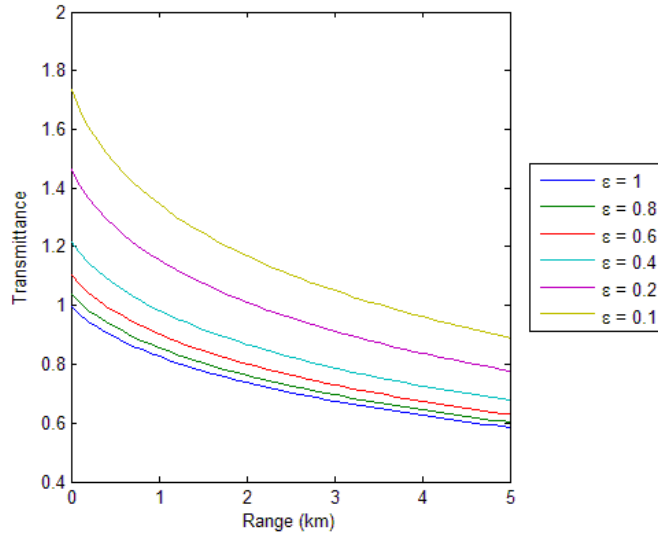


Figure 20: Curves of growth as calculated by the algorithm for different continuum factors ϵ . These curves were generated by simulating the observed signal using different values for ϵ and using the algorithm to compute a transmittance spectrum. This computed transmittance spectrum was then used to develop the curves of growth

The difference in transmittance between a perfect blackbody spectrum and one with a continuum factor of 0.6 is 0.03, which comes to an error in transmittance of 5%.

To see how this error in transmittance affected range estimates, the derivative of the inverse of the curve of growth for the perfect blackbody was calculated. This resultant curve gives error in range as a function of error in transmittance. This curve was then multiplied by an error in transmittance to yield error in range as a function of range:

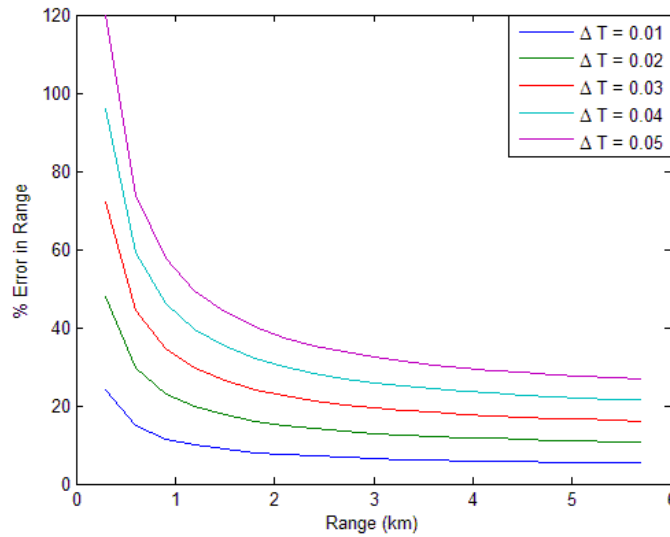


Figure 21: Error in range as a function of range for different errors in transmittance. Even small errors in transmittance can produce large errors in range estimates

Most of the experimental data was taken at a range of approximately 4 km. The derivative of the curve of growth at this range was calculated to be about 24 km / uncertainty in transmittance.

$$\left. \frac{ds}{dt} \right|_{4km} = 24km \quad (34)$$

As stated earlier, an uncertainty in ϵ of 0.4 yields an uncertainty in transmittance of 0.03.

As a result, the error in range turns out to be 17%. From this, it is evident that the continuum factor alone is enough to account for the systematic error observed in the range estimates for the graybody method. If ϵ could be calculated to within 10% however, it would not be unreasonable to assume an uncertainty in transmittance of 0.01 (figure 20). This would yield an error in range of 6%. Other sources of error include detector noise or random error in computing the baseline. These are not thought to be significant compared to the previously mentioned factors, however.

Discussion

As indicated by the data, selective emission within the absorption band cannot be completely neglected. The amount of selective emission that is present within the absorption band is determined by the continuum factor ϵ . While this did not appear to have any significant effect on range estimates for the two-band method, this may have been due to incorrect assumptions made about the source spectrum. For example, if water concentrations in the fireball were much higher than predicted, then there would be a great amount of emission in the blue region unaccounted for, which would add a negative bias to the range estimate. The same would be true if there were an emitting specie that was unaccounted for which corrupted the absorption estimate for the blue band. One other possibility would be that the correction for absorption due to water was faulty. Since water concentrations are highly variable in the atmosphere and probably also in the fireball, and the effect of emission and absorption due to water are heavily weighted towards the blue region of the absorption band, it is not surprising that utilizing the red band alone yielded more accurate results. Even though the red band is weaker and more susceptible to errors in transmittance, use of this band eliminates many of the factors which contribute to error. One caveat is the accuracy of the CO₂ concentration estimate for the source. While this technique worked for the certain type of explosive material used, it may have been coincidental. Even though the explosives used for the Eglin test would have provided a control for this variable, the data was collected at a range where errors were too high to give any conclusive evidence for or against the method presented. Future work will be needed to provide a more definitive answer.

VI. Conclusion

The method presented in this study detailed how to extract range by examining atmospheric absorption due to the 2.0 μm CO_2 band. By working through Schwarzschild's equation for radiative transfer, a model was developed for predicting the apparent intensity observed by the detector. Under the assumption that the target being ranged has an emission spectrum dominated by continuum, the unattenuated signal can be de-coupled from the attenuated signal. Examples of such targets would include reentry vehicles and solid rocket motors that have a sizeable amount of particulate in the plume. This method is predicted to be most useful for an airborne sensor looking downward. Validation was performed using an experimental setup less optimal than the downward viewing geometry. The experimental data consisted of spectra for 23 high explosive events using a horizontal viewing geometry at ground elevation. Using a graybody assumption for the source, a systematic error of 13% was observed, resulting in an under-estimation of the true range. This error was likely caused by emission within the absorption band. Using certain order of magnitude assumptions for the spatial extent, temperature, and CO_2 and water concentrations of the detonation fireball, a correction for spectrally selective emission was obtained. Those assumptions were based on previous research which investigated CO_2 and H_2O concentrations in the fireballs of high explosive detonations[10]. The correction used unattenuated emission data from one band and unattenuated gray body emission from another to determine the graybody factor. This correction factor seemed to be connected with the type of explosive used, indicating that this factor can be exploited in addition to range. Range estimates accounting for emission consistently produced results with an error of about 3%.

Future Work

While results for the present study seem promising, much of the data used came from only one type of explosive material, albeit in various quantities. A stronger case for this method can be made if it is successfully applied to a wider range of targets. Spectra for solid rocket fuel would be ideal, since that would truly define the scope of this technique.

The possibility exists that the method presented in this study, as it stands now, will prove inadequate for use against targets such as missiles. Even so, there will still be ISR applications for reentry vehicles, since the spectra of such targets should closely resemble that of a blackbody. The scope of this method can also be significantly broadened, to possibly include aircraft, provided there was a way to gain certain information on the target. Current research at AFIT aims to classify high explosive events using a 4 or 5 band method. If such a method could be developed for a wider class of targets, then temperature, CO₂, and water concentrations could be determined using a 4-band radiometer. Those parameters could then be used as inputs to account for emission within the absorption band. Using a radiometer that utilizes multiple narrow band-pass filters (about 10 nm to capture the absorption band) a passive ranging device could be developed at a reasonable cost.

Final Remarks

A technique which determines range to target using a passive method such as the one presented in this study can provide numerous benefits to future operations. Since passive techniques require less power than active ones, they can be more readily incorporated with air- and space-borne assets. If integrated with space-borne assets that

typically rely on multi-sensor triangulation for determining target location, the size of the constellation can be reduced. This technique can also enhance the capabilities of a missile defense network. Boost-phase trajectories could be determined by purely passive systems that have access to areas where radar coverage is denied. This technique would also prevent low observable platforms from having to use an active technique such as radar which would reveal position.

While there is yet to be any conclusive evidence for the successful application of this technique against a broad range of targets, initial results seem promising. Order of magnitude estimates for parameters which govern source emission seem to be adequate. If future work indicates that more fidelity is required for other target classes, there are still opportunities to couple this method with other techniques that characterize the target using low cost methods.

Appendix A. Pre-Processing Algorithm

Description: The following algorithm was used to determine which frames should be used for optimization. Qualitative inspection of the subsequent plots allows the user to select the frames.

```
start=1;
nd=11;
[r,c]=find(y==max(y(1:end-1,300)));
plot(x,y(r+start:r+nd,:))

i=x>=2615&x<=2730;
yH2O=y(r+start,i); xH2O=x(i);

i=x>=4655&x<=5020;
yCO2=y(r+start:r+nd,i); xCO2=x(i);
[r,c]=size(yCO2);
y2=zeros(r,c);
i=xCO2<=4810|(xCO2>=4895&xCO2<=4925);
xeps=xCO2(i); yeps=yCO2(:,i);
for j = 1:r
    c=polyfit(xCO2(i),yCO2(j,i),1);
    y2(j,:)=yCO2(j,:)./polyval(c,xCO2);
end
i=(xCO2>=4810&xCO2<=4895)|(xCO2>=4925&xCO2<=5010);
x2=xCO2(i); y2=y2(:,i);
plot(x2,y2)
mean(std(y2))
```

Appendix B. Instrument Line Shape Algorithm

The following algorithm was created by Dr. Kevin Gross. The author has not made any modifications or additions to the program.

Description: A high resolution spectrum and instrument parameters are input. An inverse Fourier transform is performed on the high resolution data and convolved with an instrument lineshape specified by the user. The spectrum is then re-created using the result, allowing for a proper comparison to be made between model spectra and data.

```
function [X,Y,x,y] = FTS_ILS_conv(X,Y,L,apod,Xout)
% [X,Y] = FTS_ILS_conv(X,Y,MOPD[,apod,Xout])
%
% Convolve high-res (monochromatic) spectrum with FTS instrument
% lineshape
% function. By default, the ILS is a sinc function. Apodization
% functions
% can be applied. The resolution of the FTS is determined by the
% maximum
% optical path difference (MOPD).
%
% --- Inputs ---
% X      - input spectral axis [1/cm]
% Y      - corresponding spectrum [arb.]
% MOPD   - maximum optical path difference [cm]
% apod*  - (optional) apodization function
%         (rect,triangle,hamming,hanning)
% Xout*  - (optional) output spectral axis [1/cm]
%
% --- Outputs ---
% Y2     - spectrum convolved with ILS

% Standardize vector sizes
X = X(:);
Y = Y(:);

% Extend spectrum to be of even length
len = length(X);
if ~mod(len,2)
    len2 = len;
else
    len2 = len+1;
end
```

```

dX = X(2)-X(1);
if nargin > 4
    ix = X > min(Xout) & X < max(Xout);
else
    ix = true(size(X));
end
sf1 = trapz(X(ix),Y(ix));
X(len+1:len2) = X(len)+[1:len2-len]*dX;
Y(len+1:len2) = Y(len);

% Determine ILS scanning function to use
if nargin < 4, apod = 'rect'; end
dX = X(2)-X(1);
Lm = 1/dX;
x = (Lm/len2) * ([len2/2:len2-1 0:len2/2-1] - (len2/2) ); % x axis
built so that fftshift is unnecessary
switch lower(apod)
    case {'tri','triangle','bartlet'} % Triangle
        ILSfft = apod_tri(x,L);
    case {'hamming','ham'} % Hamming
        ILSfft = apod_hamming(x,L);
    case {'hanning','hann','han','cosine','cos'} % Hanning
        ILSfft = apod_hann(x,L);
    case {'rectangle','rect','sinc'} % No apodization
        ILSfft = apod_rect(x,L);
    otherwise
        ILSfft = apod_rect(x,L);
        warning('Unknown apodization function - defaulting to sinc
(rectangle)');
end

% Do convolution using built-in fft
if nargout > 2, y = fft(Y).*ILSfft'; end
Y = ifft(fft(Y).*ILSfft');
X = X(1:len);
Y = Y(1:len);
if nargin > 4
    try
        Y = interp1f(X,Y,Xout); % Use mex file if it exists
    catch
        Y = interp1(X,Y,Xout,'linear'); % Otherwise use built-in
interp1
    end
    X = Xout;
    sf2 = trapz(X,Y);
    Y = Y * sf1 / sf2;
else
    Y = Y * sf1 / trapz(X,Y);
end

% -----
% Apodization functions
% -----

```

```

function ILSfft = apod_rect(x,L)
ILSfft = abs(x) <= L;

function ILSfft = apod_tri(x,L)
ILSfft = zeros(size(x));
ix = abs(x) <= L;
ILSfft(ix) = 1-abs(x(ix)/L);

function ILSfft = apod_hamming(x,L)
ILSfft = zeros(size(x));
ix = abs(x) <= L;
c1 = 0.428752;
ILSfft(ix) = ( 1+2*c1*cos(pi*x(ix)/L) ) / (1+2*c1);

function ILSfft = apod_hann(x,L)
ILSfft = zeros(size(x));
ix = abs(x) <= L;
ILSfft(ix) = ( 1+cos(pi*x(ix)/L) ) / 2;

```

Appendix C. Water Correction Algorithm

Description: Data taken from the 2615-2730 cm^{-1} region is used as the input. The output is proportional to the concentration length. The proportionality constant is taken into account in the CO_2 fitting algorithm

```
function c = H2O_fit(x,y)
%x0
%1-2 - polynolmial coefficients
%3   - water correction

cs_dir='C:\Users\Douglas\Documents\Workspace\Cross Sections\';
load([cs_dir,'H2O cross section.mat']);

N=1.0133E5/(1.3807E-23*300);
xx=x; yy=linspace(0,0.02,20);
[X,Y]=meshgrid(xx,yy);

MOPD=1/(2*mean(diff(x)));
apod='rect';

Z=zeros(length(yy),length(xx));
for i = 1:length(yy)
    [T1,T2]=FTS_ILS_conv(nu,exp(-yy(i)*N*H2O_cs*4E3),MOPD,apod,x);
    Z(i,:)=T2(:);
end

y=real(y);
xxi=x;
yyi=@(x0) repmat(x0,1,length(x));
I=@(x0,x) polyval(x0(1:2),x).*interp2(X,Y,Z,xxi,yyi(x0(3)));
%I2=@(x0,x) I(x0,x)/max(I(x0,x));
%I=@(x0,x) polyval(x0(1:2),x).*Zi(x0(3));

x0(1:2)=polyfit(x,y,1);
x0(3)=0.002;
options=optimset('LargeScale','off');
warning off all
c=lsqcurvefit(I,x0,x,y,[],[],options);
plot(x,I(c,x),x,y);
c=c(3);
```

Appendix D. Continuum Factor Optimization Routine

Description: Data starting from the beginning of the baseline (4655 cm^{-1}) to the end of the CO_2 absorption band (5020 cm^{-1}) is used as an input. The model for the continuum factor is calculated as outlined in chapter VI.

```
function c = eps_fit(x,y)

cs_dir='C:\Users\Douglas\Documents\Workspace\HighTemp Cross Sections\';
load([cs_dir,'H2O cross section.mat']);
load([cs_dir,'CO2 cross section.mat']);

[X,Y]=meshgrid(nu,temperature);
[xxi,yyi]=meshgrid(nu,1000);
CO2=interp2(X,Y,CO2_cs,xxi,yyi);
H2O=interp2(X,Y,H2O_cs,xxi,yyi);

xx=x; yy=linspace(0,0.95,20);
[X,Y]=meshgrid(xx,yy);

MOPD=1/(2*mean(diff(x)));
apod='rect';

Z=zeros(length(yy),length(xx));
for i = 1:length(yy)
    T=(1-yy(i)*exp(-10^23*H2O*10).*exp(-10^23*CO2*10));
    [T1,T2]=FTS_ILS_conv(nu,T,MOPD,apod,x);
    j=T1<=4810;
    c=polyfit(T1(j),T2(j),1);
    T2=T2./polyval(c,T1).*1/(1-yy(i));
    Z(i,:)=T2(:);
end

y=real(y);
[r,c]=size(y);
y2=zeros(r,c);
i=x<=4810;
for j = 1:r
    c=polyfit(x(i),y(j,i),1);
    y2(j,:)=y(j,:)./polyval(c,x);
end
y2=mean(y2);
i=x>=4895&x<=4925;
x2=x(i); y2=y2(i);
```

```
xxi=x2;
yyi=@(x0) repmat(x0,1,length(x2));
I=@(x0,x2) interp2(X,Y,Z,xxi,yyi(x0));
%I=@(x0,x) polyval(x0(1:3),x).*Zi(x0(4));

x0=.01;
options=optimset('LargeScale','off');
warning off all
c=lsqcurvefit(I,x0,x2,y2,[],[],options);
plot(x2,I(c,x2),x2,y2);
```

Appendix E. CO₂ Optimization Routine

Description: Data starting from the beginning of the baseline (4655 cm⁻¹) to the end of the CO₂ absorption band (5020 cm⁻¹) is used as an input, as well as the water and continuum correction factor. Pressure and temperature are manually adjusted in the m-file. A 1 parameter fit using MATLAB's built in Levenberg-Marquardt least squares fitting algorithm is used to output range.

```
function c = CO2_fit2(x,y,epsilon,W)

cs_dir='C:\Users\Douglas\Documents\Workspace\HighTemp Cross Sections\';
load([cs_dir,'H2O cross section.mat']);
load([cs_dir,'CO2 cross section.mat']);

[X,Y]=meshgrid(nu,temperature);
[xxi,yyi]=meshgrid(nu,1000);
CO2=interp2(X,Y,CO2_cs,xxi,yyi); %#ok<NODEF>
H2O=interp2(X,Y,H2O_cs,xxi,yyi); %#ok<NODEF>

[X,Y]=meshgrid(nu,temperature);
[xxi,yyi]=meshgrid(nu,300);
CO2_cs=interp2(X,Y,CO2_cs,xxi,yyi);
H2O_cs=interp2(X,Y,H2O_cs,xxi,yyi);

N=1.0133E5/(1.3807E-23*300);
xx=x; yy=linspace(0,6,20);
[X,Y]=meshgrid(xx,yy);

MOPD=1/(2*mean(diff(x)));
apod='rect';

Z=zeros(length(yy),length(xx));
for i = 1:length(yy)
    T=exp(-W*N*H2O_cs*4E3).*exp(-367*1E-6*N*CO2_cs*yy(i)*1E3)...
        .* (1-epsilon*exp(-10^23*H2O*10).*exp(-10^23*CO2*10));
    [T1,T2]=FTS_ILS_conv(nu,T,MOPD,apod,x);
    j=T1<=4810;
    c=polyfit(T1(j),T2(j),1);
    T2=T2./polyval(c,T1).*1/(1-epsilon);
    Z(i,:)=T2(:);
end
```

```

y=real(y);
[r,c]=size(y);
y2=zeros(r,c);
i=x<=4810;
for j = 1:r
    c=polyfit(x(i),y(j,i),1);
    y2(j,:)=y(j,:)./polyval(c,x);
end
y2=mean(y2);
i=(x>=4810&x<=4895) | (x>=4925&x<=5010);
x2=x(i); y2=y2(i);

xxi=x2;
yyi=@(x0) repmat(x0,1,length(x2));
I=@(x0,x2) interp2(X,Y,Z,xxi,yyi(x0));
%I=@(x0,x) polyval(x0(1:3),x).*Zi(x0(4));

x0=4;
options=optimset('LargeScale','off');
warning off all
c=lsqcurvefit(I,x0,x2,y2,[],[],options);
plot(x2,I(c,x2),x2,y2);

```

Bibliography

- [1] A. Jursa (ed), *Handbook of Geophysics and the Space Environment.*: Air Force Geophysics Laboratory, 1985.
- [2] James Stark et al. Draper, "Airborne validation of an IR passive TBM ranging sensor," *Proceedings of SPIE*, vol. 3698, pp. 491-500, April 1999.
- [3] Gordon Scriven and Nahum Gat, "Advanced Monocular Passive Ranging (AMPR) for HALO II," Opto-Knowledge Systems Inc., Torrance, CA, SBIR Phase II Final Report AFRL-PR-ED-TR-2008-0018, 2008.
- [4] Hawks M et al., "Short Range Demonstrations of Passive Ranging," Air Force Institute of Technology, Wright-Patterson Air Force Base,.
- [5] N. Gat et al., "Advanced Monocular Passive Ranging," Opt-Knowledge Systems Inc., Torrance, CA, SBIR Phase I Final Report AFRL-PR-ED-TR-2003-0001, 2003.
- [6] Grant W. Petty, *A First Course in Atmospheric Radiation*. Madison, WI: Sundog Publishing, 2004.
- [7] Jay A. Orson, "Collection of Detonation Signatures and Characterization of Spectral Features," Air Force Institute of Technology, Wright-Patterson Air Force Base, Thesis AFIT/GSO/ENP/00M-01, 2001.
- [8] William J. Miller and Sean C. Miller, "Radiant Brass Phase 3B Test Report," SciTec, Princeton, Test Report 1999.
- [9] Joe Motos Gordon, Glenn P. Perram, and Kevin C. Gross, "Temporally-Resolved, Infrared Spectra from the Detonation of Advanced Munitions," Air Force Institute of Technology, Wright-Patterson Air Force Base,.
- [10] Kevin Gross, "Phenomenological Model for Infrared Emissions from High-Explosive Detonation Fireballs," Air Force Institute of Technology, Wright Patterson Air Force Base, Dissertation AFIT/DS/ENP/07-03, 2007.
- [11] Tracy H. Jackson, "An Analytical Model for Predicting the Radiation from Jet Plumes in the Mid-Infrared Spectral Region," Army Missile Command, Redstone Arsenal, AL, AD871980 1970.

REPORT DOCUMENTATION PAGE				<i>Form Approved OMB No. 074-0188</i>	
<p>The public reporting burden for this collection of information is estimated to average 1 hour per response, including the time for reviewing instructions, searching existing data sources, gathering and maintaining the data needed, and completing and reviewing the collection of information. Send comments regarding this burden estimate or any other aspect of the collection of information, including suggestions for reducing this burden to Department of Defense, Washington Headquarters Services, Directorate for Information Operations and Reports (0704-0188), 1215 Jefferson Davis Highway, Suite 1204, Arlington, VA 22202-4302. Respondents should be aware that notwithstanding any other provision of law, no person shall be subject to a penalty for failing to comply with a collection of information if it does not display a currently valid OMB control number.</p> <p>PLEASE DO NOT RETURN YOUR FORM TO THE ABOVE ADDRESS.</p>					
1. REPORT DATE (DD-MM-YYYY) 25-03-2010		2. REPORT TYPE Master's Thesis		3. DATES COVERED (From - To) March 2002 - March 2003	
TITLE AND SUBTITLE Passive Ranging Using Infra-Red Atmospheric Attenuation				5a. CONTRACT NUMBER	
				5b. GRANT NUMBER	
				5c. PROGRAM ELEMENT NUMBER	
6. AUTHOR(S) Macdonald, Douglas J., Captain, USAF				5d. PROJECT NUMBER F4FTAX9224J001	
				5e. TASK NUMBER	
				5f. WORK UNIT NUMBER	
7. PERFORMING ORGANIZATION NAMES(S) AND ADDRESS(S) Air Force Institute of Technology Graduate School of Engineering and Management (AFIT/ENY) 2950 Hobson Way, Building 640 WPAFB OH 45433-8865				8. PERFORMING ORGANIZATION REPORT NUMBER AFIT/GAP/ENP/10-M09	
9. SPONSORING/MONITORING AGENCY NAME(S) AND ADDRESS(ES) National Air and Space Intelligence Center Attn: Nathan Sutters 4180 Watson Way Wright Patterson AFB, OH 45433 (937) 255-4493				10. SPONSOR/MONITOR'S ACRONYM(S) NASIC/DAPM	
				11. SPONSOR/MONITOR'S REPORT NUMBER(S)	
12. DISTRIBUTION/AVAILABILITY STATEMENT APPROVED FOR PUBLIC RELEASE; DISTRIBUTION UNLIMITED.					
13. SUPPLEMENTARY NOTES					
14. ABSTRACT Methods of estimating range to an emissive target based on the depth of an atmospheric absorption band are demonstrated. The present work uses measurements of the CO2 absorption band centered at 2.0 μm where signal-to-background ratios are maximum for many applications. Model results, based on high-resolution transmission molecular absorption (HITRAN) database cross sections, are used to predict range accuracy at ranges of up to 50 km and are compared with short range (<5km) experimental results. The spectra of 23 high explosive events were used to validate the model. Using the assumption of a blackbody spectrum, extracted ranges consistently underestimated the true range by approximately 13%. By incorporating the stoichiometry of the fireball from previous research and using particulate contribution as a parameter, the error for the range estimates could be reduced to 3%.					
15. SUBJECT TERMS Passive Ranging, Remote Sensing					
16. SECURITY CLASSIFICATION OF:			17. LIMITATION OF ABSTRACT	18. NUMBER OF PAGES	19a. NAME OF RESPONSIBLE PERSON
a. REPORT	b. ABSTRACT	c. THIS PAGE			19b. TELEPHONE NUMBER (Include area code)
U	U	U	UU	66	Michael R. Hawks, LtCol, USAF (ENP) (937) 255-3636, x4828 michael.hawks@afit.edu

Standard Form 298 (Rev. 8-98)
Prescribed by ANSI Std. Z39-18